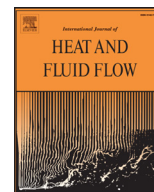




Contents lists available at ScienceDirect

## International Journal of Heat and Fluid Flow

journal homepage: [www.elsevier.com/locate/ijheatfluidflow](http://www.elsevier.com/locate/ijheatfluidflow)

# Large-scale motions in a turbulent channel flow with the slip boundary condition

Min Yoon<sup>a</sup>, Jinyul Hwang<sup>a</sup>, Jin Lee<sup>a</sup>, Hyung Jin Sung<sup>a,\*</sup>, John Kim<sup>b</sup>

<sup>a</sup> Department of Mechanical Engineering, KAIST, 291 Daehak-ro, Yuseong-gu, Daejeon 34141, Republic of Korea

<sup>b</sup> Mechanical and Aerospace Engineering Department, UCLA 48-121, Engineering 4, UCLA, Los Angeles, CA 90095-1597, United States

## ARTICLE INFO

Article history:  
Available online xxx

Keywords:  
Large-scale motions  
Slip boundary condition  
Footprints  
Drag reduction

## ABSTRACT

Direct numerical simulation (DNS) of a turbulent channel flow with the slip boundary condition was performed to investigate the spatial characteristics of large-scale motions (LSMs) in a drag-reducing flow and the influence of LSMs on drag reduction. The slip boundary condition was applied in the streamwise direction. DNS of a channel flow with the no-slip boundary condition was also conducted for comparison. The overall mean skin-friction coefficient of the flow with the slip boundary condition was reduced by 35% relative to the flow with the no-slip condition at the same bulk Reynolds number of 10,333. The streamwise and spanwise length scales of the LSMs in the outer region are larger with the slip boundary condition than with the no-slip condition due to a large population of long LSMs. These LSMs influence the near-wall region via roll-cell motions and footprints. Although the number of total streaks decreases, a portion of the footprints increases due to the influence of the outer LSMs. The streamwise vorticities around the low-speed footprints are attenuated more than those around the high-speed footprints. The LSMs and the near-wall footprints contribute 45% of the total reduction in the skin friction coefficient, with 25% of this contribution due to low-speed LSMs.

© 2016 Elsevier Inc. All rights reserved.

## 1. Introduction

Turbulent flows are composed of coherent structures on a multiplicity of scales that range from the viscous length scale  $\delta_\nu$  ( $\equiv \nu/u_\tau$ ) near the wall, where  $\nu$  and  $u_\tau$  are the kinematic viscosity and friction velocity respectively, to the outer length scale  $\delta$ . Beyond the log layer, the large-scale motions (LSMs) of length scale  $\delta$  are bulges or groups of hairpin vortices with a streamwise alignment (Adrian, 2007). LSMs have crucial roles in momentum transfer and in the generation of turbulent kinetic energy in the outer region (Ganapathisubramani et al., 2003; Liu et al., 2005; Guala et al., 2006; Balakumar and Adrian, 2007; Hutchins and Marusic, 2007a; Lee and Sung, 2011). Since LSMs contribute significant portion of the entire streamwise kinetic energy and the Reynolds shear stress, the characteristics and influences of LSMs are important to the analysis of turbulent phenomena. Moreover, they influence the surrounding flow, especially the near-wall streamwise velocity fluctuations. Hutchins and Marusic (2007a) analyzed turbulent boundary layer flows at various friction Reynolds numbers and found that the outer peak of the streamwise long wavelength appears in

the log layer and that these LSMs have influences on the near-wall region known as footprints. In addition, the large-scale structures modulate the small-scale near-wall energy. Mathis et al. (2009) introduced the amplitude modulation coefficient, which is the degree of amplitude modulation of near-wall streamwise velocity fluctuations by large-scale structures. Counter-rotating roll motions have been observed in the conditionally averaged flow fields around large-scale streamwise fluctuations in the log layer (Hutchins and Marusic, 2007b; Chung and McKeon, 2010; Baltzer et al., 2013). The counter-rotating roll motions produced by the large-scale structures influence the near-wall fluctuations and contribute to the reduction in the skin-friction drag.

Turbulent drag produces adverse effects on the energy efficiency and performance of many systems. Thus, drag reduction in wall-bounded turbulent flows can result in significant economic savings (Park and Sung, 2001). For example, a decrease of 30% in fuel consumption on shipping industries worldwide via drag reduction would lead to savings of \$38 billion per year (Kim, 2011). Several means of reducing turbulent drag have been studied, such as the use of hydrophobic surfaces in passive control methods. The slip occurring over such a hydrophobic surface leads to drag reduction because of the weakened mean-shear rate. Increased attention has been paid to hydrophobic surfaces to optimize drag reduction and to verify the drag reduction mechanism. Note that

\* Corresponding author. Tel.: +82 42 350 3027; fax: +82 42 350 5027.  
E-mail address: [hjsung@kaist.ac.kr](mailto:hjsung@kaist.ac.kr) (H.J. Sung).

<http://dx.doi.org/10.1016/j.ijheatfluidflow.2016.03.003>

S0142-727X(16)30019-4/© 2016 Elsevier Inc. All rights reserved.

near-wall motions are self-sustained through the formation among the streamwise vorticities, streaks and streamwise-dependent disturbances (Hamilton et al., 1995; Waleffe, 1997; Kim, 2011). Accordingly, most research into drag reduction through the creation of hydrophobic surfaces has focused on near-wall behavior. However, since large-scale coherent structures play a crucial role in the turbulent production and momentum transfer, it is also essential to analyze the LSMs in turbulent channel flows with slip phenomena. Moreover, an improved understanding of the behavior of large-scale coherent structures in turbulent channel flows with the slip boundary condition could provide insights into drag-reduced turbulent flows and improve our control of turbulent flows.

Direct numerical simulations (DNSs) have been performed for turbulent channel flows with the slip boundary condition to mimic hydrophobic surfaces. Min and Kim (2004) conducted DNSs of fully developed turbulent channel flows at a friction Reynolds number,  $Re_\tau$ , of 180 with the Navier slip boundary condition (Navier, 1823), where the slip phenomena occurred entirely on the wall. When only streamwise slip occurs, a decrease of streamwise vorticities ( $\omega_x$ ) results in drag reduction. Spanwise slip was found to intensify the streamwise vorticities and to result in an increase in drag. After this pioneering study, Martell et al. (2009) applied an inhomogeneous wall condition to a turbulent channel flow by introducing ridge and post geometries that modeled side-by-side air-pocket interfaces. They found an overlap of the Reynolds shear stress profiles near the hydrophobic surfaces, which suggests that the near-wall turbulence structures are not fundamentally altered by this approach. Their results are in agreement with experimental data obtained for a ridge spacing of  $30 \mu\text{m}$  by Daniello et al. (2009). Martell et al. (2010) performed DNSs with the inhomogeneous wall condition and found that the hydrophobic features affect the near-wall region up to a distance less than or equal to the feature spacing in the wall units. Their results for the instantaneous streamwise and wall-normal velocity fluctuations indicate that the turbulent structures are simply shifted toward the hydrophobic wall by the hydrophobic features. Park et al. (2013) showed that drag reduction in laminar channel flows is constant for a fixed geometry and various Reynolds numbers. The drag reduction in turbulent channel flows is a function of the effective slip length when it is normalized by the inner scale. The maximum drag reduction is obtained by decreasing the number of streamwise vortices near the hydrophobic wall. Jelly et al. (2014) reported that a small population of vortical structures in the buffer layer is associated with a reduction in the turbulent drag via a weakening of the Q2 and Q4 events. Many studies have focused on the surface geometries and behavior of near-wall structures, e.g. streamwise vorticities and vortical structures, to optimize drag reduction. However, further analysis is required to explain the roles of turbulent structures in drag reduction, particularly that of long coherent structures.

The objectives of the present study were to investigate the influence of LSMs in the outer region on the drag reduction associated with near-wall behavior. The DNS of a turbulent channel flow with the slip boundary condition was performed. The spatial features of the LSMs were explored to determine their role in drag reduction. The slip boundary condition was used to determine the relative importance to drag reduction of the coherent structures in the turbulent flow. For comparison, the DNS of a turbulent channel flow with the no-slip condition was also conducted. The friction Reynolds numbers of the channel flows with the slip and no-slip conditions were 469 and 577 respectively. The turbulence statistics of the flows were compared to validate the data and to characterize the effects of the slip condition on the turbulence structures. Conditional two-point correlations and conditionally averaged velocities were employed to examine the role of the LSMs in drag

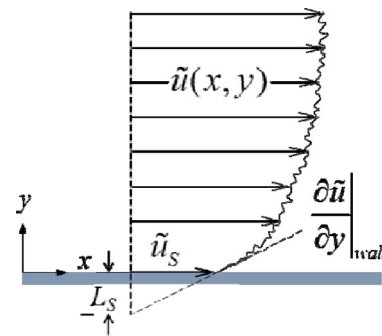


Fig. 1. Schematic diagram of a streamwise velocity profile.

reduction. Finally, the skin-friction coefficient was decomposed to determine the contributions of the LSMs to drag reduction.

## 2. Numerical simulation

The non-dimensional governing equations for an incompressible flow are

$$\frac{\partial \tilde{u}_i}{\partial t} + \frac{\partial \tilde{u}_i \tilde{u}_j}{\partial x_j} = -\frac{\partial \tilde{p}}{\partial x_i} + \frac{1}{Re_b} \frac{\partial^2 \tilde{u}_i}{\partial x_j \partial x_j}, \quad (1)$$

and

$$\frac{\partial \tilde{u}_i}{\partial x_i} = 0, \quad (2)$$

where  $x_i$  are the Cartesian coordinates and  $\tilde{u}_i$  are the corresponding velocity components ( $\tilde{u}_i \equiv U_i + u_i$ ). The notational convention adopted is that  $x$ ,  $y$ , and  $z$  denote the streamwise, vertical, and spanwise coordinates, respectively, and that  $u$ ,  $v$ , and  $w$  denote the velocity fluctuations of the corresponding directions. Each term in the governing equations was normalized by the bulk velocity ( $U_b$ ) and the channel half-height ( $\delta$ ). The Reynolds number ( $Re_b \equiv U_b \delta / \nu$ ) was 10,333. The governing equations were solved by using the fully implicit fractional step method to decouple the velocity and pressure. The convection and viscous terms were discretized in time implicitly by using the second-order Crank-Nicolson scheme. All terms were discretized in space by using the second-order central difference scheme with a staggered grid. Details of the numerical procedure can be found in Kim et al. (2002).

The periodic boundary condition was applied to the streamwise and spanwise directions. The Navier slip boundary condition was applied at both walls  $\tilde{u}_s \equiv L_s (\partial \tilde{u} / \partial y)|_{\text{wall}}$ , where  $\tilde{u}_s$  and  $L_s$  are the slip velocity and the slip length respectively, in order to mimic a hydrophobic surface. Fig. 1 shows a schematic diagram of a streamwise velocity profile and its relationship with the slip boundary condition. The slip length was set to 0.01 to obtain a drag reduction rate of 35% in the reference channel flow with the no-slip condition (expected  $Re_\tau = 550$ ). A theoretical equation relating the drag reduction rate and the friction Reynolds number was used to determine the slip length (Fukagata et al., 2006). The friction Reynolds numbers ( $Re_\tau \equiv u_\tau \delta / \nu$ ) for the slip and no-slip boundary conditions were 469 and 577, respectively. Hereafter, the sub/superscript "0" indicates that the quantity is normalized by the inner variables of the no-slip condition, i.e. the friction velocity  $u_{\tau 0}$  and the viscous length scale  $\delta_{\nu 0} (\equiv \nu / u_{\tau 0})$ . A very long computational domain, 30 times longer than the channel half-height, was adopted in order to resolve the large-scale structures. The computation domain sizes ( $L_x$ ,  $L_y$ , and  $L_z$ ) were  $10\pi\delta$ ,  $2\delta$ , and  $3\pi\delta$  in the streamwise, wall-normal, and spanwise directions, respectively. The dimensions of the grid were 2497 ( $x$ ), 401 ( $y$ ), and 1249 ( $z$ ). The uniform grid spacings in the wall-parallel plane were  $\Delta x^{+0} \approx 7.27$  and  $\Delta z^{+0} \approx 4.36$ , and the grids in the wall-normal direction

Download English Version:

<https://daneshyari.com/en/article/4993274>

Download Persian Version:

<https://daneshyari.com/article/4993274>

[Daneshyari.com](https://daneshyari.com)